Earthq Eng & Eng Vib (2021) 20: 553-565 **DOI**: https://doi.org/10.1007/s11803-021-2038-3

Efficient seismic analysis for nonlinear soil-structure interaction with a thick soil layer

Gao Zhidong[1†], Zhao Xu[1‡], Zhao Mi[1§], Du Xiuli[1§], Wang Junjie[2§] and Liu Pengcheng[1†]

1. *Key Laboratory of Urban Security and Disaster Engineering of Ministry of Education, Beijing University of Technology, Beijing 100124, China*

2. *College of Civil Engineering, Tongji University, Shanghai 200092, China*

Abstract: The direct finite element method is a type commonly used for nonlinear seismic soil-structure interaction (SSI) analysis. This method introduces a truncated boundary referred to as an artificial boundary meant to divide the soil-structure system into finite and infinite domains. An artificial boundary condition is used on a truncated boundary to achieve seismic input and simulate the wave radiation effect of infinite domain. When the soil layer is particularly thick, especially for a three-dimensional problem, the computational efficiency of seismic SSI analysis is very low due to the large size of the finite element model, which contains an whole thick soil layer. In this paper, an accurate and efficient scheme is developed to solve the nonlinear seismic SSI problem regarding thick soil layers. The process consists of nonlinear site response and SSI analysis. The nonlinear site response analysis is still performed for the whole thick soil layer. The artificial boundary at the bottom of the SSI analysis model is subsequently relocated upward from the bottom of the soil layer (bedrock surface) to the location nearest to the structure as possible. Finally, three types of typical sites and underground structures are adopted with seismic SSI analysis to evaluate the accuracy and efficiency of the proposed efficient analysis scheme.

Keywords: soil-structure interaction; thick soil layer; efficient analysis; absorbing boundary

1 Introduction

Soil-structure interaction (SSI) (Wolf, 1985, 1988; Casciati and Borja, 2004; Emani and Maheshwari, 2009; Manna and Baidya, 2010; Carbonari *et al*., 2011; Luo and Yang, 2016; Zhao *et al*., 2017; Abel *et al*., 2018; Huang *et al*., 2020; Li *et al*., 2020) significantly affects seismic response of many kinds of civil infrastructures, such as underground structures, high dams, nuclear power plants, large-span bridges and so on. Numerical analysis of seismic SSI is an important step in the performance-based design of the above-mentioned structures. The direct finite element method (Wolf, 1985, 1988) is often adopted for such analysis. In this process, one-dimensional (1D) seismic site response analysis is initially completed and next an SSI analysis is carried out for a truncated SSI model. An absorbing boundary condition is used for the truncated boundary of the SSI analysis model to simulate the wave radiation effect of infinite domain. Finally, the equivalent seismic load obtained from the site response is applied to achieve seismic input (Zhao *et al*., 2017; Huang *et al*., 2017; Huang *et al*., 2018).

Material nonlinearity behavior is usually found in soil under earthquake loads. The same constitutive models of soils in the site response analysis model and the SSI analysis model should be used in order to obtain more reasonable and precise results. However, the 1D seismic site response analysis was often performed by employing the linear elastic model (Zhao *et al*., 2017; Huang *et al*., 2018), the equivalent linear model (Schnabel *et al*., 1972; Bardet *et al*., 2000), or the hysteretic material model (Matasovic, 2006) due to the convenience of using these models. On the other hand, nonlinear SSI analysis (Zhao *et al*., 2017; Huang *et al*., 2017, 2018) was often performed by using elastic-plastic constitutive models of soils. This approach may cause significant errors due to the inconsistency of material models of soils between site response and SSI analysis. On the other hand, the absorbing boundary condition is a type of numerical method used to simulate wave radiation from a near field to a far field. Nearly all existing absorbing boundary conditions (Lysmer and Kuhlemeyer, 1969; Liao and Wong, 1984; Deeks and Randolph, 1994; Liu *et al*., 2006; Zhao *et al*., 2018a, 2018b) are only applicable to linear wave propagation problems in the far field, which

Correspondence to: Zhao Mi, Key Laboratory of Urban Security and Disaster Engineering of Ministry of Education, Beijing University of Technology, Beijing 100124, China
Tel: +86-15901456360
E-mail: zhaomi@bjut.edu.cn

[†]PhD; [‡]Assistant Professor; [§]Professor

Supported by: National Basic Research Program of China under Grant No. 2015CB057902, Ministry of Education Innovation Team of China under Grant No. IRT_17R03 and National Natural Science Foundation of China under Grant Nos. 51421005 and 51678015

Received December 17, 2019; **Accepted** August 9, 2020

means there is no appropriate boundary condition with regard to material nonlinearity in far field-related problems.

Furthermore, if shallow-buried underground structures are constructed in a thick soil layer, such as at depths between 200 m to 300 m, the computational cost of nonlinear SSI analysis will increase more than that for the structure in a thin soil layer, especially in three-dimensional (3D) cases. As a result, some efficient analysis methods were developed by reducing the calculated domain. The domain reduction method (DRM), proposed by Bielak *et al.* (2003) and applied by Yoshimura *et al.* (2003), is capable of efficiently modeling 3D wave fields for an arbitrary earthquake source in highly heterogeneous geological systems that exhibit large localized impedance contrasts and arbitrary shapes. The method uses a finite-element formulation in which the primary unknowns include the total wave field within the domain that contains the localized structure, plus a scattered wave field in the exterior domain. Recently, the substructure method (Liu *et al*., 2019; Bao *et al*., 2019) for seismic wave input in 3D dynamic soil-structure interaction analysis was also proposed, based on the direct finite element method. For example, Liu *et al*. (2019) proposed a new seismic wave input method by deducing another form of equivalent input seismic loads in the finite element model. In this new method, by imposing the displacements of the free wave field on the nodes of a substructure composed of elements with artificial boundaries, the equivalent input seismic loads were obtained through dynamic analysis of the substructure. As mentioned in the previous paragraph, these methods consider the infinite domain as linear material.

In this paper, an efficient and accurate scheme for nonlinear seismic SSI analysis pertaining to a thick soil layer is presented, based on the direct finite element method. The nonlinear site response is calculated by first using the same elastic-plastic constitutive models of soils with SSI analysis. A more accurate site response result could thereby be obtained. Next, the scattered field is approximately simulated by the viscous-spring boundary. Finally, the artificial boundary at the bottom of the SSI model is relocated upward from the actual bottom of the soil layer (bedrock surface) to reduce the calculated domain.

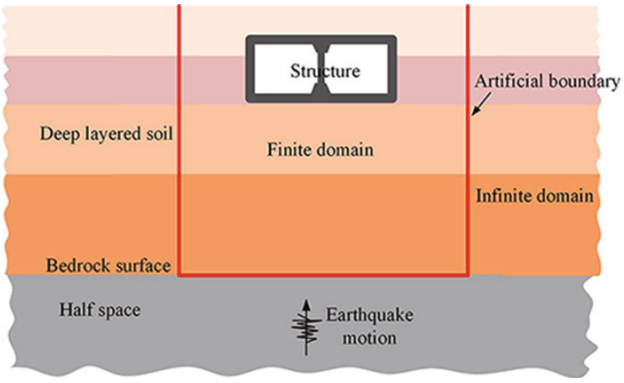

Fig. 1 Seismic soil-structure interaction problem

The remainder of this paper is organized as follows. The efficient seismic analysis scheme for nonlinear SSI with a thick soil layer is presented in Section 2. Numerical examples are provided in Section 3 to demonstrate the effectiveness of efficient nonlinear seismic SSI analysis schemes. Section 4 is the concluding section of this paper.

2 Efficient method for nonlinear seismic soil-structure interaction

2.1 Method statement

The seismic SSI problem is shown in Fig. 1. An earthquake is considered to be the vertical incident plane body wave arising from a half-space bedrock. The direct finite element method (Wolf, 1985, 1988) is one of the commonly used time history methods for nonlinear seismic SSI analysis. In this approach, a truncated boundary known as an artificial boundary is introduced to divide the soil-structure system into finite and infinite domains. The finite domain contains the structure and its adjacent soil, which is modeled using the finite element method. After the spatial discretization the finite element equation of the finite domain is:

$$\begin{bmatrix} \boldsymbol{M}_{\mathrm{RR}} & \boldsymbol{M}_{\mathrm{RB}} \\ \boldsymbol{M}_{\mathrm{BR}} & \boldsymbol{M}_{\mathrm{BB}} \end{bmatrix} \begin{Bmatrix} \ddot{\boldsymbol{u}}_{\mathrm{R}} \\ \ddot{\boldsymbol{u}}_{\mathrm{B}} \end{Bmatrix} + \begin{bmatrix} \boldsymbol{C}_{\mathrm{RR}} & \boldsymbol{C}_{\mathrm{RB}} \\ \boldsymbol{C}_{\mathrm{BR}} & \boldsymbol{C}_{\mathrm{BB}} \end{bmatrix} \begin{Bmatrix} \dot{\boldsymbol{u}}_{\mathrm{R}} \\ \dot{\boldsymbol{u}}_{\mathrm{B}} \end{Bmatrix} + \begin{Bmatrix} \boldsymbol{F}_{\mathrm{R}}(\boldsymbol{u}, \dot{\boldsymbol{u}}) \\ \boldsymbol{F}_{\mathrm{B}}(\boldsymbol{u}, \dot{\boldsymbol{u}}) \end{Bmatrix} = \begin{Bmatrix} \boldsymbol{0} \\ \boldsymbol{f}_{\mathrm{B}} \end{Bmatrix} \tag{1}$$

where the subscripts B and R denote the degrees of freedom on the artificial boundary and the remaining part of the finite domain, respectively; $\boldsymbol{u}$, $\dot{\boldsymbol{u}}$, and $\ddot{\boldsymbol{u}}$ are the absolute displacement, velocity and acceleration vectors, respectively; $\boldsymbol{M}$, $\boldsymbol{C}$ and $\boldsymbol{K}$ are the mass, damping and stiffness matrices, respectively; $\boldsymbol{F}$ denotes the nonlinear restoring force vector; and $\boldsymbol{f}_{\mathrm{B}}$ is the load vector of the infinite domain to the finite domain.

The whole field can be decomposed into free and scattered fields (Wolf, 1985, 1988) at the artificial boundary, whose procedure can be written as:

$$\boldsymbol{f}_{\mathrm{B}} = \boldsymbol{f}_{\mathrm{B}}^{\mathrm{F}} + \boldsymbol{f}_{\mathrm{B}}^{\mathrm{S}} \tag{2}$$

$$\boldsymbol{u}_{\mathrm{B}} = \boldsymbol{u}_{\mathrm{B}}^{\mathrm{F}} + \boldsymbol{u}_{\mathrm{B}}^{\mathrm{S}}, \ \dot{\boldsymbol{u}}_{\mathrm{B}} = \dot{\boldsymbol{u}}_{\mathrm{B}}^{\mathrm{F}} + \dot{\boldsymbol{u}}_{\mathrm{B}}^{\mathrm{S}} \tag{3}$$

where the superscripts F and S denote the free and scattered fields. The free field can be obtained by using site response analysis. A numerical experiment shows that the value of the free field is much higher than the scattered field. Therefore, it is essential to first guarantee the accuracy of the free field in earthquake input.

The scattered field is approximately simulated by the viscous-spring boundary (Liu *et al.*, 2006). The formulation of the viscous-spring boundary can be written as:

$$\boldsymbol{f}_{\mathrm{B}}^{\mathrm{S}} = -\boldsymbol{K}_{\mathrm{B}}^{\infty}\boldsymbol{u}_{\mathrm{B}}^{\mathrm{S}} - \boldsymbol{C}_{\mathrm{B}}^{\infty}\dot{\boldsymbol{u}}_{\mathrm{B}}^{\mathrm{S}} \tag{4}$$

where $\boldsymbol{K}_{\mathrm{B}}^{\infty}$ and $\boldsymbol{C}_{\mathrm{B}}^{\infty}$ are the stiffness and damping matrices.

Both the stiffness and damping matrices can be diagonalized using spatially lumped discretization. The viscous-spring boundary consists of a linear spring and a dashpot connected in parallel for each degree of freedom on the artificial boundary. The stiffness and damping matrices for a boundary node k can be rewritten as:

$$\boldsymbol{K}_{\mathrm{B}k}^{\infty} = \begin{bmatrix} K_{\mathrm{N}} & 0 \\ 0 & K_{\mathrm{T}} \end{bmatrix},\ K_{\mathrm{N}} = l_k \frac{1}{1+A}\frac{\lambda_n + 2G_n}{2r}$$
$$\text{and } K_{\mathrm{T}} = l_k \frac{1}{1+A}\frac{G_n}{r} \tag{5-1}$$

$$\boldsymbol{C}_{\mathrm{B}k}^{\infty} = \begin{bmatrix} C_{\mathrm{N}} & 0 \\ 0 & C_{\mathrm{T}} \end{bmatrix},\ C_{\mathrm{N}} = l_k B \rho_n c_{\mathrm{p}_n} \text{ and}$$
$$C_{\mathrm{T}} = l_k B \rho_n c_{\mathrm{s}_n} \tag{5-2}$$

where the subscripts N and T denote normal and tangent directions, respectively; ρ is the mass density of the n-th layer soil; G, c_{s} and c_{p} are the shear modulus, velocity of the shear wave, and compression wave in the medium, respectively; l_k is the coefficient due to lumped discretization; r is the distance between the wave source and the artificial boundary; A and B are the modified coefficients, which in this paper are 0.8 and 1.1, respectively.

The displacement and velocity of the scattered field are eliminated by substituting Eq. (3) into Eq. (4). Later, the equation obtained above is substituted into Eq. (2) and then into Eq. (1), and after some manipulations the finite element equation is ultimately obtained found to be:

$$\begin{bmatrix} \boldsymbol{M}_{\mathrm{RR}} & \boldsymbol{M}_{\mathrm{RB}} \\ \boldsymbol{M}_{\mathrm{BR}} & \boldsymbol{M}_{\mathrm{BB}} \end{bmatrix} \begin{Bmatrix} \ddot{\boldsymbol{u}}_{\mathrm{R}} \\ \ddot{\boldsymbol{u}}_{\mathrm{B}} \end{Bmatrix} + \begin{bmatrix} \boldsymbol{C}_{\mathrm{RR}} & \boldsymbol{C}_{\mathrm{RB}} \\ \boldsymbol{C}_{\mathrm{BR}} & \boldsymbol{C}_{\mathrm{BB}} + \boldsymbol{C}_{\mathrm{B}}^{\infty} \end{bmatrix} \begin{Bmatrix} \dot{\boldsymbol{u}}_{\mathrm{R}} \\ \dot{\boldsymbol{u}}_{\mathrm{B}} \end{Bmatrix} +$$
$$\begin{Bmatrix} \boldsymbol{F}_{\mathrm{R}}(\boldsymbol{u},\dot{\boldsymbol{u}}) \\ \boldsymbol{F}_{\mathrm{B}}(\boldsymbol{u},\dot{\boldsymbol{u}}) \end{Bmatrix} + \begin{bmatrix} \boldsymbol{0} & \boldsymbol{0} \\ \boldsymbol{0} & \boldsymbol{K}_{\mathrm{B}}^{\infty} \end{bmatrix} \begin{Bmatrix} \boldsymbol{u}_{\mathrm{R}} \\ \boldsymbol{u}_{\mathrm{B}} \end{Bmatrix} = \begin{Bmatrix} \boldsymbol{0} \\ \boldsymbol{K}_{\mathrm{B}}^{\infty}\boldsymbol{u}_{\mathrm{B}}^{\mathrm{F}} + \boldsymbol{C}_{\mathrm{B}}^{\infty}\dot{\boldsymbol{u}}_{\mathrm{B}}^{\mathrm{F}} + \boldsymbol{f}_{\mathrm{B}}^{\mathrm{F}} \end{Bmatrix} \tag{6}$$

The seismic load, $\boldsymbol{f}_{\mathrm{B}}^{\infty}$, acting on the artificial boundary, can be written from Eq. (6) as:

$$\boldsymbol{f}_{\mathrm{B}}^{\infty} = \boldsymbol{K}_{\mathrm{B}}^{\infty}\boldsymbol{u}_{\mathrm{B}}^{\mathrm{F}} + \boldsymbol{C}_{\mathrm{B}}^{\infty}\dot{\boldsymbol{u}}_{\mathrm{B}}^{\mathrm{F}} + \boldsymbol{f}_{\mathrm{B}}^{\mathrm{F}} \tag{7}$$

where $\boldsymbol{u}_{\mathrm{B}}^{\mathrm{F}}$, $\dot{\boldsymbol{u}}_{\mathrm{B}}^{\mathrm{F}}$ and $\boldsymbol{f}_{\mathrm{B}}^{\mathrm{F}}$ are the displacement, velocity and internal force of free field, respectively; the seismic load $\boldsymbol{f}_{\mathrm{B}}^{\infty}$ is referred to as the equivalent nodal load.

It can be seen from the Eq. (7) that the seismic site response analysis needs to first be calculated to obtain the displacement, velocity and internal force of the free field; subsequently, earthquake input can be achieved. The schematic diagram of the direct finite element method for seismic SSI analysis is shown in Fig. 2. When considering the material nonlinearity of soils, the same nonlinear model of soils must be used in site response analysis and SSI analysis. However, for the convenience of the program, seismic site response analysis was often performed by employing the linear elastic model (Zhao *et al.*, 2017; Huang *et al.*, 2018) or the equivalent linear model. As mentioned in the introduction of this paper, only the nonlinear model is used in finite domain. In this paper, the nonlinear site response analysis is used and presented in Section 2.2.

On the other hand, the truncated bottom boundary (earthquake input location) is often set at the bedrock surface or below the bedrock surface because the nonlinear site response can be calculated when the site is subjected to the vertical incident plane body wave arising from the half space. For a shallow structure in a thick soil layer site, the computational cost is extremely high due to the large finite element domain, especially for 3D cases. The efficient and accurate scheme developed in this paper for nonlinear seismic SSI analysis with a thick soil layer is presented in this section. As shown in Fig. 3, nonlinear seismic site response analysis is still performed using the whole thick soil layer. Site response can maintain a negligible computational cost by building the model of a column with finite elements. The details of this nonlinear site response scheme will be described in Subsection 2.2. To significantly save on the computational cost, 2D or 3D nonlinear SSI analysis is performed by using a reduced finite element model that is obtained by relocating the bottom artificial boundary upward from the bedrock surface. Earthquake input is achieved at the depth of the relocated bottom artificial boundary, which can be assumed to be rigid or flexible. A rigid bottom boundary indicates that the motion of

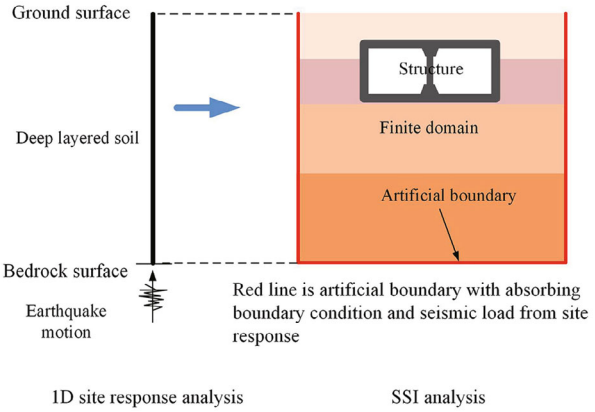

Fig. 2 Direct finite element method for seismic SSI analysis

site response at the location of the bottom boundary is directly imposed. For the treatment of the flexible bottom boundary, the displacement, velocity and internal force of site response corresponding to the bottom boundary location is used to calculate equivalent seismic load in Eq. (7), which is subsequently acted upon the bottom boundary of the SSI model. Also, the viscous-spring boundary is also used at the bottom of the model to simulate the wave radiation effect of infinite domain. A rigid bottom boundary is easier to operate than a flexible bottom boundary. This will be proved by the numerical example in which the reduced model with a flexible bottom boundary has higher degree of accuracy than that having a rigid bottom boundary.

2.2 Site response analysis

Site response analysis takes place before the SSI analysis. The same software needs to be used in both site response and SSI analysis in order to assure having the same nonlinear material models of soils. The scheme of nonlinear site response analysis based on the 2D column of finite elements is shown in Fig. 4(a). Rigid constraints (Zienkiewicz *et al*., 1988) are used at nodes of the same height. Nonlinearity of soil is considered by adopting the elastic-plastic constitutive model in finite elements. The bedrock is assumed be consist of linear elastic material, which is truncated by the artificial boundary. The viscous boundary and seismic loading from the input earthquake are applied to the artificial boundary. Site response analysis can provide nodal displacement, velocity, and internal force at the truncated boundaries for subsequent SSI analysis. The effectiveness of this scheme will be validated by numerical examples presented in Subsection 3.2.

For the efficient analysis method, before performing the nonlinear SSI analysis for the reduced finite element model, it is indicated here that the nonlinear site response, using the reduced model, is equivalent to using the whole thick soil layer model. The process is shown in Fig. 4. As shown in Fig. 4(a), the nonlinear site response is first performed using the whole thick soil layer. As shown in Figs. 4(b) and 4(c), the site response is calculated through the use of the reduced model. In Fig. 4(b), it is assumed that the artificial bottom boundary of the reduced model is flexible, where the viscous-spring boundary and the seismic load obtained from the site response of whole thick soil layer are applied, as seen in Subsection 2.1. In Fig. 4(c), the bottom artificial boundary of the reduced model is assumed to be rigid, where the displacement of site response at the bottom boundary is imposed. The site responses of Figs. 4(b) and 4(c) are equivalent to the corresponding site response shown in Fig. 4(a). This is essential for the establishment of the efficient analysis method. The process is verified by numerical examples included in Subsection 3.2. The flow chart of nonlinear SSI analysis combined with ABAQUS (2014) is shown in Fig. 5.

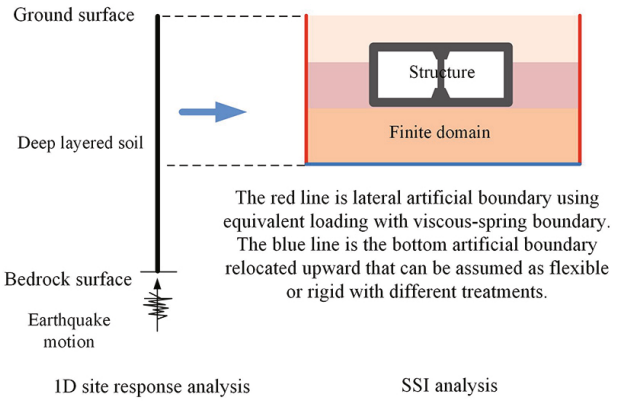

Fig. 3 Efficient analysis for seismic SSI with a thick soil layer

3 Validation of the nonlinear soil-structure interaction analysis

Compared with the whole thick soil layer, the smaller finite element domain can effectively solve this problem. However, it should be considered whether the

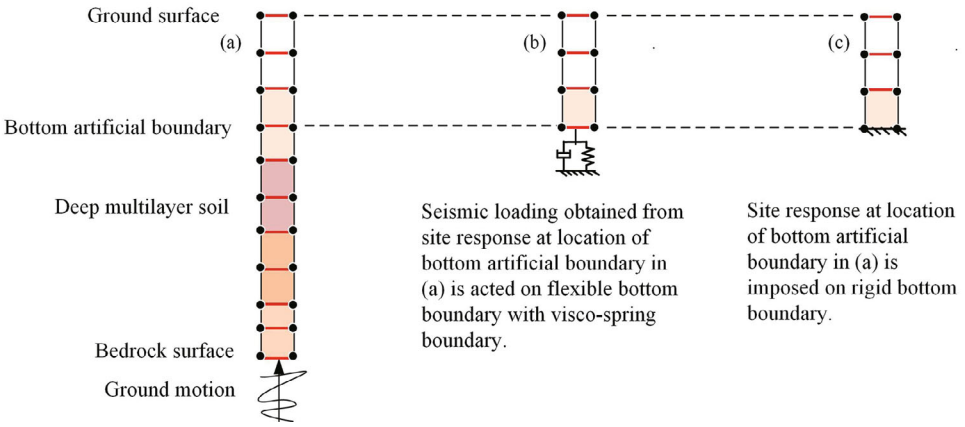

Fig. 4 Nonlinear seismic site response analysis: (a) 2D site response analysis using the whole thick soil layer; and (b) and (c) site response analyses with flexible and rigid bottom boundaries, respectively

accuracy of the scheme is satisfactory. On the one hand, as shown in Subsection 3.2, it is proven by numerical experiments that the exact site response results for the reduced model can be obtained by inputting the results of the site response of the whole soil layer. On the other hand, the accuracy of the SSI analysis using the reduced model with varied locations regarding the bottom artificial boundary should be compared with that of using the model with the whole thick soil layer. This will be addressed in Subsection 3.3.

To prove the effectiveness of the efficient seismic SSI analysis scheme for a thick soil layer, the numerical results from three case studies, including a one-story, two-span subway station; a two-story, three-span subway station; and a circle tunnel are presented in this section. Also, the efficient analysis scheme is applied to calculate the dynamic response of the 3D model of the one-story, two-span station to further demonstrate the feasibility of the efficient analysis scheme for a more complicated case study. The accuracy and efficiency of the efficient analysis scheme for the underground structure is discussed herein. The numerical analysis is implemented with the use of ABAQUS software.

3.1 Underground structures taken as examples

Three typical cross sections of underground structures with detailed geometries are shown in Fig. 6. In this figure, the red nodes and sections are used as representative nodes and sections to present calculation results. The burial depth and material properties of the structures are listed in Table 1. It should be noted that during the 2D analysis the central column is assumed to be a continuous wall (Huo *et al*., 2005). According to the equivalent method of bending stiffness, the actual spacing of the columns in the longitudinal direction is taken into consideration, with reduced section width. The actual spacing of the columns in the longitudinal direction for a one-story, two-span subway station and a two-story, three-span subway station are 3.5 m and 9.3 m, respectively. Three types of sites, from hard to soft, with a homogeneous soil layer on half-space bedrock, named Site 1, Site 2 and Site 3, were selected for this study. They belong to class II, class III and class IV, respectively, according to the Chinese Code for Seismic Design of Urban Rail Transit Structures (GB 50909–2014). The mechanical behavior of the surrounding soil is simulated by the Mohr-Coulomb constitutive model, which is characterized by cohesion, the friction angle, the elastic modulus, and the Poisson ratio. The geometry and elastic material constants of the three sites are shown in Table 2. The cohesion and friction angle of soils are 20 kPa and 5°, respectively. The bedrock is regarded to be a linear elastic material. The density and shear wave velocity of bedrock are 2100 kg/m^3 and 500 m/s, respectively.

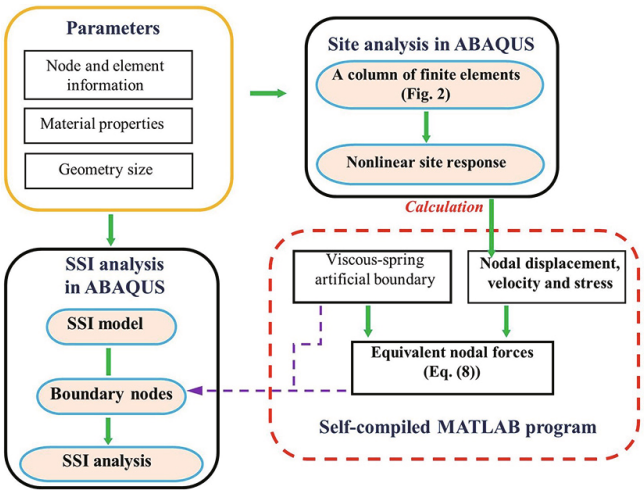

Fig. 5 Flow chart of nonlinear SSI analysis combined with ABAQUS

Therefore, three 2D SSI analysis models were built in ABAQUS as shown in Fig. 7 to validate the accuracy and efficiency of the method. The thickness of the whole thick soil layer is 250 m. The accuracy of the reduced model for the site response and SSI analyses is indicated by comparing the solution of the reduced model with that of the whole thick soil layer. The bottom boundary location of the SSI model is studied in this section. So, in order to reduce the error caused by lateral artificial boundaries, the widths of all the 2D finite element models are set to 300 m. A 4-node bilinear, reduced integration plain strain element, CPE4R, which is provided by the ABAQUS element library, is used to model the surrounding soil and subway station structure. The implicit integration algorithm is used in the software. The surrounding soil domain is discretized with a consideration of the numerical accuracy of simulating seismic wave propagation, which requires mesh size of 1/10–1/8 of the wavelength (Ma *et al*., 2018). The finite element mesh size of soils and structures are 1 m × 1 m and 0.2 m ×0.2 m, respectively, which satisfies the accuracy requirement for dynamic analysis.

Table 1 Burial depth and material properties for the three structures

Structure	Burial depth (m)	Density (kg/m^3)	Elastic modulus (GPa)	Poisson ratio	Elastic modulus of columns (GPa)
One-story two-span station	5	2500	24.0	0.18	6.85
Two-story three-span station	5	2500	32.5	0.20	3.48
Tunnel	5	2500	24.0	0.18	\

Table 2 Geometry and material constants of sites

Site names	Site classification	Thickness (m)	Density (kg/m^3)	Shear wave velocity (m/s)
Site 1	II	250	1900	300
Site 2	III	250	1900	250
Site 3	IV	250	1900	150
Bedrock	–	250–∞	2100	500

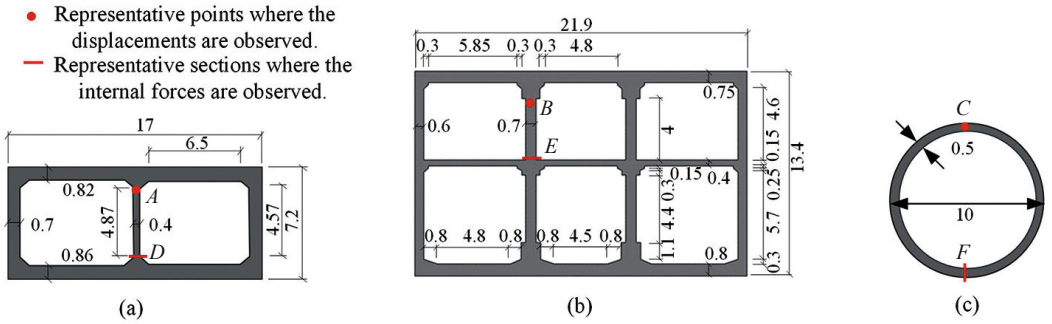

Fig. 6 Three kinds of underground structures: (a) one-story, two-span subway station; (b) two-story, three-span subway station; and (c) circle tunnel. The unit of length is m

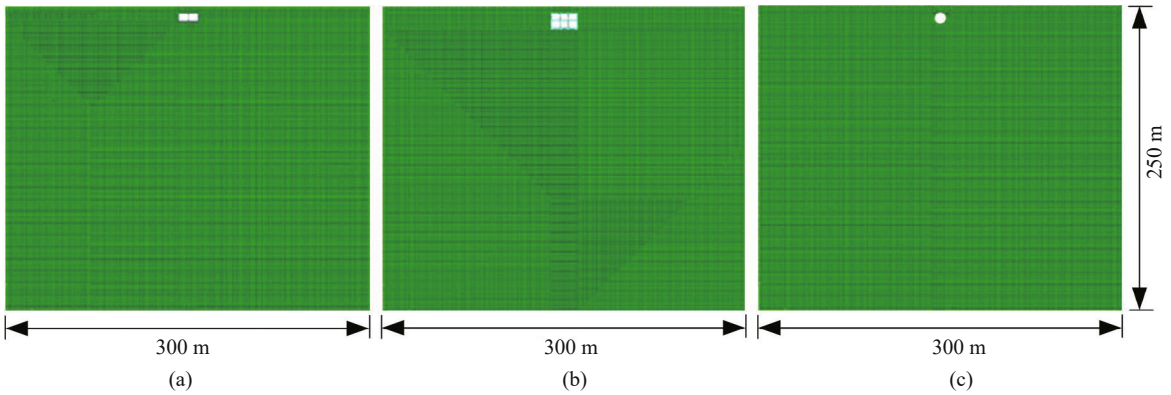

Fig. 7 Finite element models of SSI systems: (a) one-story, two-span station with Site 1, Site 2 and Site 3, respectively; (b) two-story, three-span station with Site 1, Site 2 and Site 3, respectively; and (c) tunnel with Site 1, Site 2 and Site 3, respectively

An earthquake is inputted as a vertically incident SV wave from the underlying half-space bedrock. The incident earthquake motion from the half-space bedrock is half of the bedrock outcrop motion according to wave theory when assuming the bedrock is a linear elastic material. So, the Kobe University record obtained from the bedrock outcrop is lessened as half to input, and the modified acceleration time history and its response spectrum is shown in Fig. 8.

3.2 Site response analysis results

The effectiveness of the nonlinear site response analysis scheme presented in Subsection 2.2 is initially indicated here by numerical examples. Also, the site responses shown in Figs. 4(b) and 4(c) are equivalent to the corresponding site response of Fig. 4(a), which is also verified in this section.

In order to prove the accuracy of these solutions, a reference solution is given via the finite element analysis of an adequately large model so that the wave reflection from the lateral boundary does not affect the site response at the central line of the model. The maximum shear wave velocity of soil (300 m/s) multiplies the required computational time (8.8 s) to arrive at the distance from the lateral boundary to the central line of the model. Therefore, the width of the reference model is 5300 m, and the mesh size of the finite element is illustrated in Fig. 9.

The nonlinear site response results are shown in Fig. 10. The reference solution is obtained by computing the reference model between the beginning 0–8 s because the reference model can obtain an accuracy solution within 8 s. The result of entire site shows that the 250 m thick soil layer is used in the site response analysis. The results of reduced sites show that only the 50 m thick

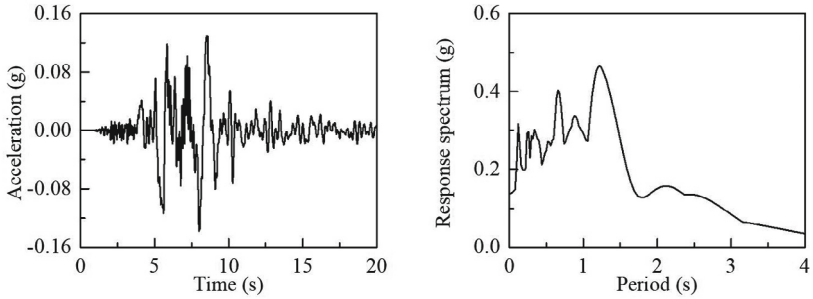

Fig. 8 Acceleration time histories of incident earthquake motion and its response spectrum

soil layer is used in site response analysis. The bottom of the reduced site is treated by flexible or rigid bottom artificial boundaries, respectively. The detailed process is presented in Subsection 2.2, Fig. 4. It can be seen from Fig. 10 that these nonlinear site responses are in agreement with the reference solution. The results also demonstrate that the efficient analysis method is accurate for the free field (site response). This is essential for the establishment of efficient analysis method.

3.3 2D SSI analysis results

When the efficient nonlinear SSI analysis is performed for a reduced finite element model, the site responses are exact as mentioned in above subsection, but they are approximate for the SSI analysis due to their approximation for the scattered field. It is difficult to provide an accuracy evaluation in theory for the reduced SSI model by comparing it to the SSI model, including the whole thick soil layer. The accuracy of the efficient SSI analysis will therefore be evaluated by the numerical experiments.

In this section, the calculation accuracy and efficiency of the efficient analysis scheme for the 2D nonlinear SSI analysis are studied. The reduced models with the flexible and rigid bottom artificial boundaries also are discussed. The bottom artificial boundary is located at depths of 20 m, 30 m, 50 m and 70 m, respectively. The solution obtained using the SSI model with the whole soil layer is provided as a reference. The thickness of the whole soil layer is 250 m, as shown in Fig. 7. For conciseness, only the dynamic responses of the representative nodes and sections of each model are plotted.

As shown in Fig. 6, points *A*, *B* and *C* are selected as representative nodes. Points *D*, *E* and *F* are selected as representative sections. The displacements of those nodes, the shear force and the bending moment of sections were extracted from the numerical analyses for comparison purposes. Also, a relative error of peak values is defined in order to quantize the accuracy of these solutions. It is written as:

$$\mathrm{PVE} = \frac{\left||r(t)|_{\max} - |r_0(t)|_{\max}\right|}{|r_0(t)|_{\max}} \tag{8}$$

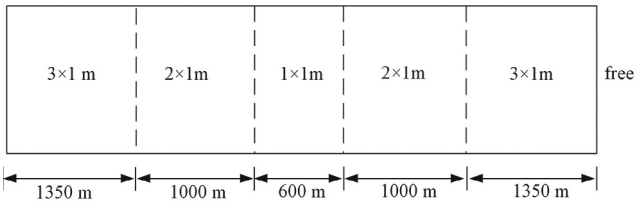

Fig. 9 Sketch for mesh size of the finite element for the reference solution

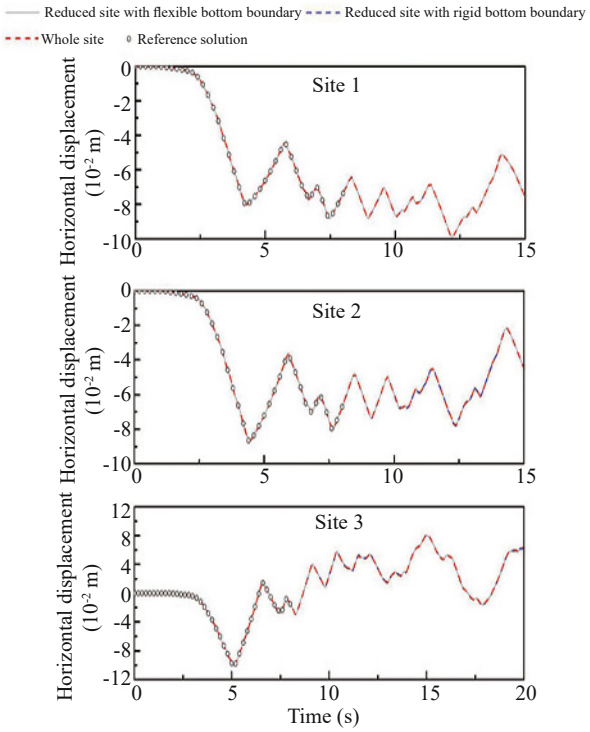

Fig. 10 Nonlinear site response results at the ground surface using Site 1, Site 2 and Site 3, respectively

where $r_0(t)$ is the reference solution; $r(t)$ is the result obtained using the reduced SSI models; | | denotes taking the absolute value; and the subscript max represents taking the maximum value.

Seismic responses of those structures at Sites 1, 2 and 3 that are under earthquake motion (Fig. 8) are shown in Figs. 11–13, respectively. The bottom artificial boundary is located at depths of 20 m, 30 m, 50 m, 70 m and 250 m, respectively. In these figures, the abbreviations RFBB

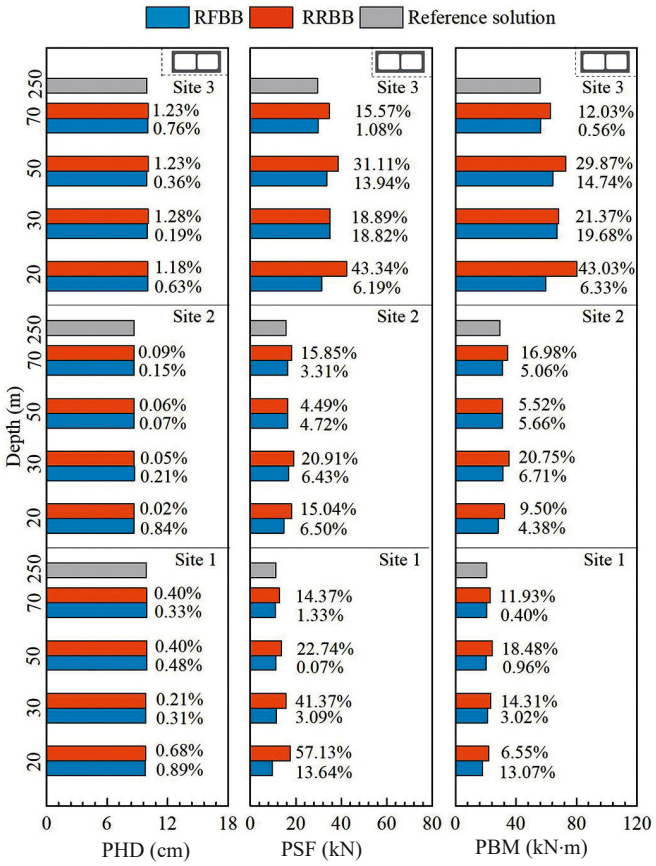

Fig. 11 Nonlinear SSI results for a one-story, two-span station structure with Site 1, Site 2 and Site 3, respectively

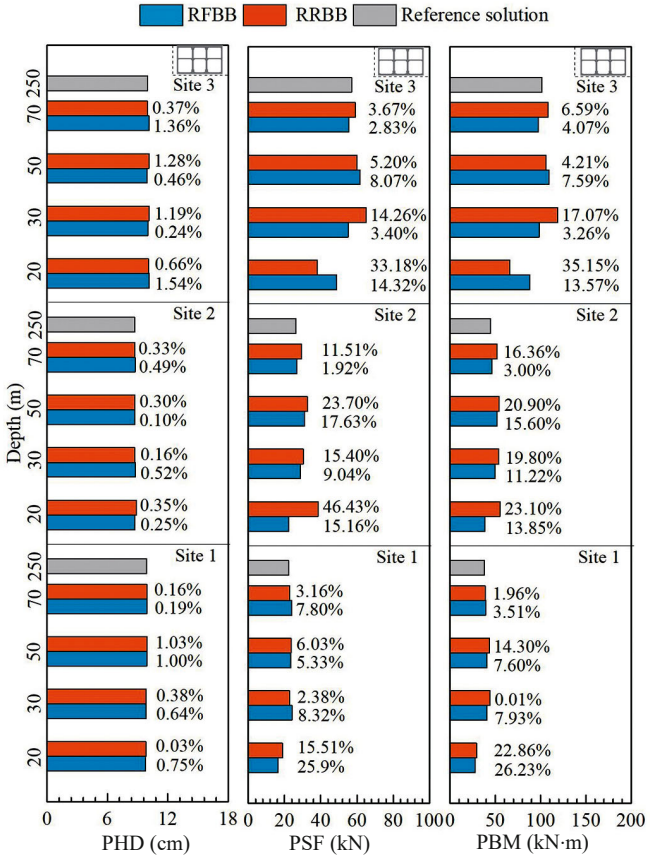

Fig. 12 Nonlinear SSI results for a two-story, three-span station structure with Site 1, Site 2 and Site 3, respectively

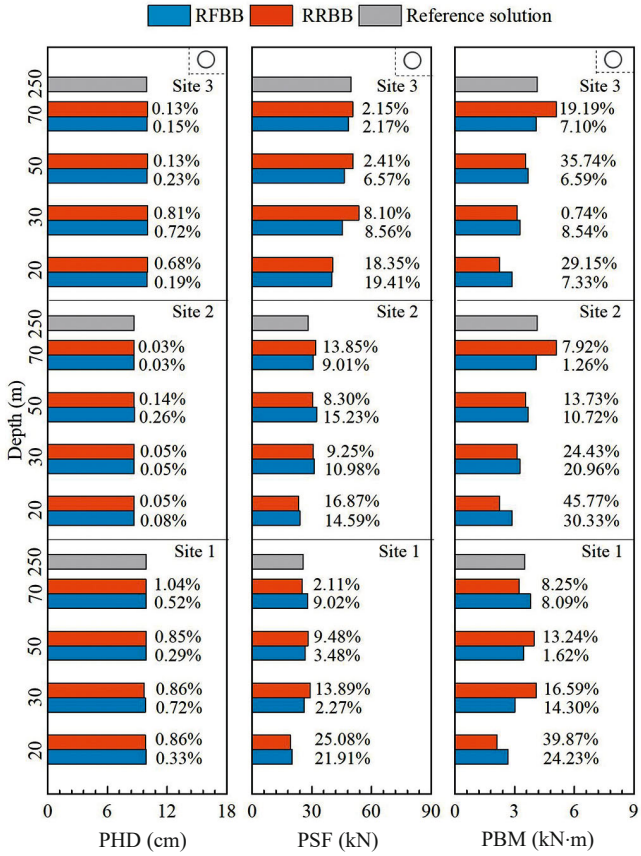

Fig. 13 Nonlinear SSI results for a tunnel with Site 1, Site 2 and Site 3, respectively

and RRBB denote the results obtained from reduced the SSI model, with a flexible bottom boundary and a rigid bottom boundary, respectively. PHD denotes the peak value of the time history of horizontal displacement; PSF and PBM denote the peak value of the time history of shear force and bending moment, respectively. The numbers at the side of the striped columns denote the error in Eq. (8) between the SSI results, using the reduced models and the reference solution.

Some conclusions can be drawn from these figures, as follows. 1) The errors of peak value displacement between reduced SSI models and the reference solution are less than 2% for all cases, which indicates that the efficient analysis scheme has high accuracy for displacement results. 2) The errors of peak value shear force and the bending moment of the reduced SSI models with a flexible bottom artificial boundary have a higher degree precision than that of the rigid bottom artificial boundary because the used visco-spring boundary can approximately absorb the scattered field. Therefore, it is recommended to use the reduced model with the flexible bottom artificial boundary. 3) The error of the peak value shear force and the bending moment of reduced SSI models with the flexible bottom artificial boundary is less than 20% when the distance from the bottom boundary of the model to the bottom of the structure exceeds twice the height of the structure. The error is less than 10% for most cases when the distance from the bottom boundary of model to the bottom of the structure exceeds 5 times the height of the structure.

In order to further evaluate the accuracy of the efficient analysis method, the spectral accelerations of representative nodes for the reduced SSI models and reference models are compared, as shown in Fig. 14. The flexible bottom artificial boundary is used in the reduced SSI models. Several conclusions can be drawn from these figures as follows. 1) The spectral accelerations of representative nodes obtained from the reduced SSI models agree well with the reference solution when Site 1 and Site 2 are used. This demonstrates that the accuracy of the efficient analysis method is higher for the relative hard site. 2) The spectral accelerations at the zero period for the five SSI models have a high degree of consistency, which indicates that peak ground acceleration (PGA) at the representative nodes obtained from the reduced SSI models have a relatively high accuracy. 3) The spectral accelerations of representative nodes with the soft Site 3 have an obvious amplification at the 1.2 s period. This also may be related to the relative low frequency of Site 3 in addition to the input earthquake motion.

For 2D SSI analysis, the number of working CPUs of a computer is 2 and the time step length is 10^{-4}. The implicit algorithm is used. Computational time consumption is shown in Table 3. It can be seen that when the depth of the bottom artificial boundary is 70 m, the computational time consumption of the efficient scheme is only 1/5 of that for the scheme using the whole thick soil layer.

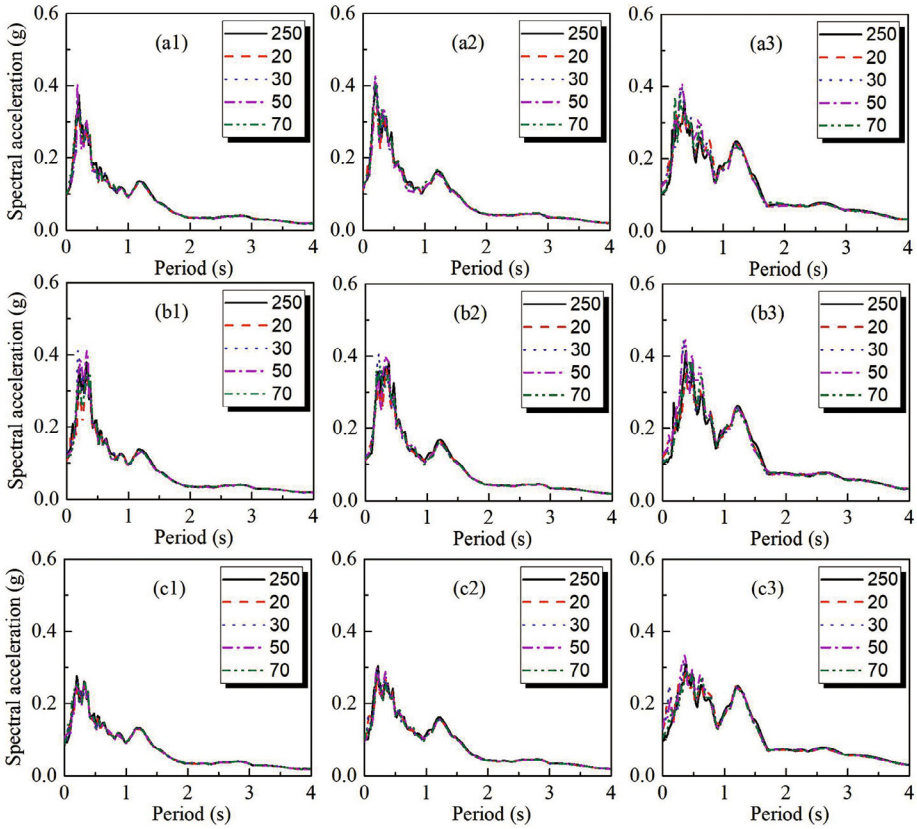

Fig. 14 Spectral accelerations of representative nodes for reduced SSI models and reference models. The flexible bottom artificial boundary is used in the reduced SSI models. (a1)–(a3) denote a one-story, two-span station structure at Site 1, Site 2 and Site 3, respectively; (b1)–(b3) denote a two-story, three-span station structure at Site 1, Site 2 and Site 3, respectively; (c1)–(c3) denote a circle tunnel structure at Site 1, Site 2 and Site 3, respectively

Table 3 Computational time for 2D SSI

Depth of model (m)	250	70	50	30	20
Number of elements	79559	23939	17759	11579	8489
Number of nodes	77158	22798	16758	10718	7698
Computational time (min)	240	50	30	20	18

3.4 3D SSI analysis results

Section 3.3 assesses the accuracy of the method used by employing the 2D SSI analysis model. The 3D SSI analysis of the one-story, two-span subway station with multiple soil layers is used to study the efficiency of the method. The geometric dimension of the structure is shown in Fig. 15. The longitudinal width of the central column of the station is 1m, with a column spacing of 2.5 m. The site conditions, including the geometry and material parameters for each soil layer and the bedrock are listed in Table 4. The Mohr-coulomb constitutive model of soils was chosen for the purpose of validating this method. The Cohesion stress and Friction angle of soils are 10 kPa and 5°, respectively. The soil with a shear wave velocity 500 m/s is regarded as the linear elastic bedrock half-space. The schematic diagram of the 3D finite element model of the soil-structure system is shown in Fig. 16. The length and width of the 3D finite element model are 67 m and 100 m, respectively. The mesh size of the finite element of soils and structures are 2 m × 2 m and 0.2 m × 0.2 m, respectively.

The bottom artificial boundary of the efficient scheme for 3D analysis is set at a depth of 30 m. The flexible bottom artificial boundary is used. The vertical earthquake motion, as shown in Fig. 8, is considered. The result of 3D analysis is shown in Fig. 17. The peak value error of displacement is less than 1%.

For 3D SSI analysis, the number of working CPUs of a computer is 8 in the ABAQUS software, and the time step length is 10^{-4}. The explicit algorithm is used. Computational time consumption is shown in Table 5. It can be seen that the computational time consumption for the efficient scheme is only the 1/3 of that of the scheme using the whole thick soil layer.

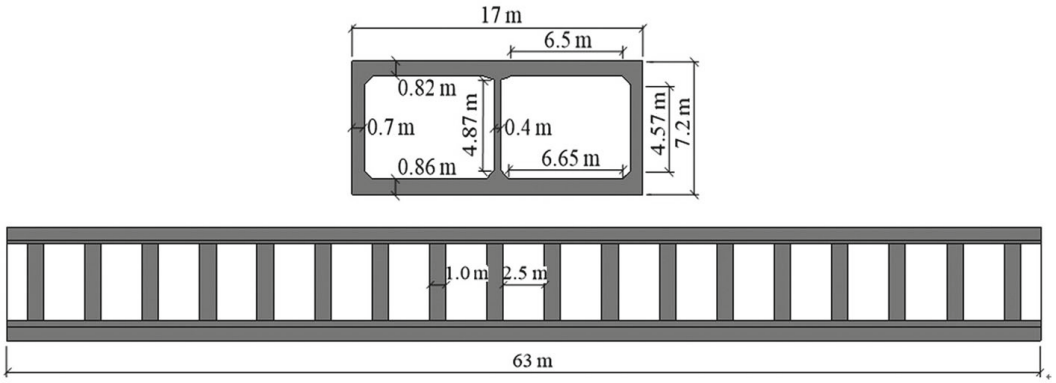

Fig. 15 Geometry constants of structure

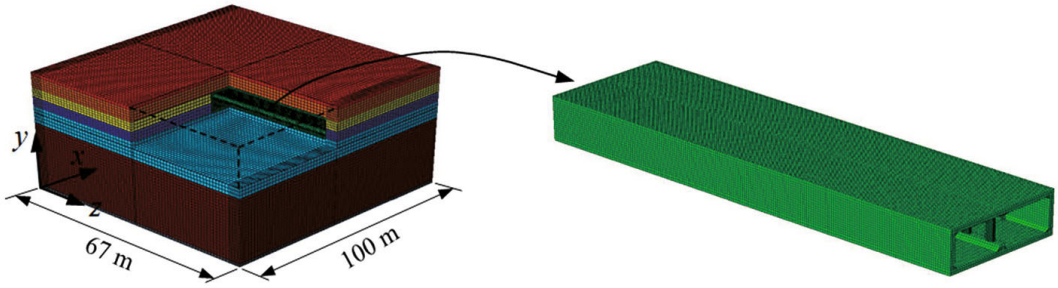

Fig. 16 Schematic diagram of the finite element model of a soil-structure system

Table 4 Geometry and material constants of soil and bedrock

Layer number	Depth (m)	Density (kg/m^3)	Shear wave velocity (m/s)	Poisson ratio
1	0–10	1900	140	0.33
2	10–30	1900	140	0.32
3	30–60	1900	170	0.32
4	60–100	1900	190	0.40
5	100–150	1900	240	0.30
6	150–250	2000	330	0.26
7	250–∞	2100	500	0.47

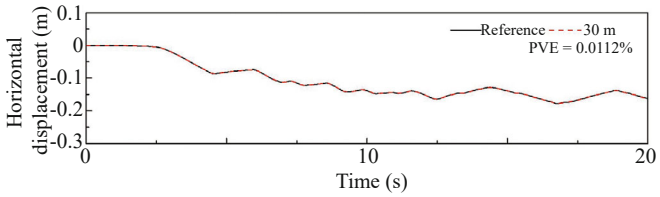

Fig. 17 3D nonlinear SSI results of the middle point of the central column of the structure. The 30 m denotes the heights of the reduced SSI model with a flexible bottom boundary. Reference solution is obtained using a whole model of 250 m depth. PVE denotes peak value error

4 Conclusions

An accurate and efficient scheme is presented to improve the computational efficiency of nonlinear SSI analysis with a shallow structure in a thick soil layer. Nonlinear site response analysis is still performed for the whole thick soil layer. Next, the bottom artificial boundary of the SSI model is subsequently relocated upward from the actual soil layer bottom (the bedrock surface). Numerical examples are given to evaluate the accuracy and efficiency of the proposed efficient

Table 5 Computational time for 3D SSI

Depth of model (m)	250	30
Number of elements	523626	33026
Number of nodes	608226	391086
Computational time (min)	900	300

analysis scheme. Some conclusions and engineering recommendations are drawn as follows.

1) The errors of peak value displacement using the reduced model are less than 2%, which indicates that the scheme has a high degree of accuracy for displacement results. 2) The errors of peak shear force and bending moment using the reduced model with a flexible bottom artificial boundary have a higher degree of precision than that with a rigid bottom boundary because the employed viscous-spring boundary can approximately absorb the scattered field. It is recommended to use the reduced model with the flexible bottom artificial boundary. 3) The error of peak value shear force and the bending moment of reduced SSI models with a flexible bottom artificial boundary is less than 20% when the distance from the bottom boundary of the model to the bottom of the structure exceeds twice the height of the structure. The error is less than 10% in most cases when the distance from the bottom boundary of the model to the bottom of the structure exceeds 5 times the height of the structure. 4) The computational cost saves about 66% for 3D SSI analyses when the bottom artificial boundary moves from a depth of 250 m to 30 m, while the computational error of peak displacement is less than 1%. Also, it should be noted that the efficient scheme does not consider the horizontal inhomogeneous soil layer or multi-point earthquake motion input at the bottom boundary of the model.

Acknowledgement

This work is supported by the National Basic Research Program of China (2015CB057902), the Ministry of Education Innovation Team of China (IRT_17R03) and the National Natural Science Foundation of China (51421005 and 51678015). Opinions and positions expressed in this paper are those of the authors only and do not reflect those of the NBRPC or the NSFC.

References

ABAQUS (2014), *Users Manual* (version 6.14-1), Providence, RI: Dassault Systemes Simulia Corp.

Abel JA, Orbović N, McCallen DB and Jeremic B (2018), "Earthquake Soil-Structure Interaction of Nuclear Power plants, differences in Response to 3-D, 3 × 1-D, and 1-D Excitations," *Earthquake Engineering and Structural Dynamics*, **47**(6): 1478–1495.

Bao X, Liu JB, Wang DY, Li ST, Wang F and Wang XF (2019), "Modification Research of the Internal Substructure Method for Seismic Wave Input in Deep Underground Structure-Soil Systems," *Shock and Vibration*, **2019**: 5926410.

Bardet JP, Ichii K and Lin CH (2000), *A Computer Program for Equivalent-Linear Earthquake Site Response Analysis of Layered Soil Deposits User's Manual*, Los Angeles: University of Southern California.

Bielak J, Loukakis K, Yoshiaki H and Yoshimura C (2003), "Domain Reduction Method for Three-Dimensional Earthquake Modeling in Localized Regions, Part I: Theory," *Bulletin of the Seismological Society of America*, **93**(2): 817–824.

Casciati S and Borja RI (2004), "Dynamic FE Analysis of South Memnon Colossus Including 3D Soil-Foundation-Structure Interaction," *Computers and Structures*, **82**(20): 1719–1736.

Carbonari S, Morici M, Dezi F and Leoni G (2011), "Seismic Soil-Structure Interaction in Multi-Span Bridges: Application to a Railway Bridge," *Earthquake Engineering and Structural Dynamics*, **40**(11): 1219–1239.

Deeks AJ and Randolph MF (1994), "Axisymmetric Time-Domain Transmitting Boundaries," *Journal of Engineering Mechanics*, **120**(1): 25–42.

Emani PK and Maheshwari BK (2009), "Dynamic Impedances of Pile Groups with Embedded Caps in Homogeneous Elastic Soils Using CIFECM," *Soil Dynamics and Earthquake Engineering*, **29**(6): 963–973.

GB 50909–2014 (2014), *Code for Seismic Design of Urban Rail Transit Structures*, China Planning Press, Beijing. (in Chinese)

Ghandil M and Behnamfar F (2015), "The Near-Field Method for Dynamic Analysis of Structures on Soft Soils Including Inelastic Soil-Structure Interaction," *Soil Dynamics and Earthquake Engineering*, **75**(1): 1–17.

Huang JQ, Zhao M and Du XL (2017), "Non-linear Seismic Responses of Tunnels Within Normal Fault Ground Under Obliquely Incident P Waves," *Tunnelling and Underground Space Technology*, **61**: 26–39.

Huang JQ, Zhao M, Xu, CS, Du XL, Jin L and Zhao X (2018), "Seismic Stability of Jointed Rock Slopes Under Obliquely Incident Earthquake Waves," *Earthquake Engineering and Engineering Vibration*, **17**(3): 527–539.

Huang JQ, Zhao X, Zhao M, Du XL, Wang Y, Zhang CM and Zhang CY (2020), "Effect of Peak Ground Parameters on the Nonlinear Seismic Response of Long Lined Tunnels," *Tunnelling and Underground Space Technology*, **95**: 103175.

Huo H, Bobet A, Fernandez G and Ramirez J (2005), "Load Transfer Mechanisms Between Underground Structure and Surrounding Ground: Evaluation of the Failure of the Daikai Station," *Journal of Geotechnical and Geoenvironmental Engineering*, **131**(12): 1522–1533.

Li L, Jiao HY, Du XL and Shi PX (2020), "Fully Fluid-Solid Coupling Dynamic Model for Seismic Response of Underground Structures in Saturated Soils," *Earthquake Engineering and Engineering Vibration*, **19**(2): 257–268.

Lysmer J and Kuhlemeyer RL (1969), "Finite Dynamic Model for Infinite Media," *Journal of the Engineering Mechanics Division*, **95**(4): 859–878.

Liao ZP and Wong HL (1984), "A Transmitting Boundary for the Numerical Simulation of Elastic Wave Propagation," *International Journal of Soil Dynamics and Earthquake Engineering*, **3**(4): 174–183.

Liu JB, Du YX, Du XL, Wang ZY and Wu J (2006), "3D Viscous-Spring Artificial Boundary in Time Domain," *Earthquake Engineering and Engineering Vibration*, **1**(5): 93–101.

Liu JB, Bao X, Wang DY, Tan H and Li ST (2019), "The Internal Substructure Method for Seismic Wave Input in 3D Dynamic Soil-Structure Interaction Analysis," *Soil Dynamics and Earthquake Engineering*, **127**: 105847.

Liu JB, Tan H, Bao X, Wang DY and Li ST (2019), "Seismic Wave Input Method for Three-Dimensional Soil-Structure Dynamic Interaction Analysis Based on the Substructure of Artificial Boundaries," *Earthquake Engineering and Engineering Vibration*, **18**(4): 747–758.

Luo C and Yang C (2016), "Nonlinear 3D Finite Element Analysis of Soil-Pile-Structure Interaction System Subjected to Horizontal Earthquake Excitation," *Soil Dynamics and Earthquake Engineering*, **84**(1): 145–156.

Matasovic N (2006), "D–MOD 2: A Computer Program for Seismic Response Analysis of Horizontally Layered Soil Deposits, Earthfill Dams and Solid Waste Landfills," *Geomotions*, LLC, Lacey, WA, USA.

Manna B and Baidya DK (2010), "Dynamic Nonlinear Response of Pile Foundations Under Vertical Vibration-Theory Versus Experiment," *Soil Dynamics and Earthquake Engineering*, **30**(6): 456–469.

Ma C, Lu DC and Du XL (2018), "Seismic Performance Upgrading for Underground Structures by Introducing Sliding Isolation Bearings," *Tunnelling and Underground Space Technology* **74**: 1–9.

Schnabel PB, Lysmer J and Seed HB (1972), "SHAKE: A Computer Program for Earthquake Ground Response Analysis for Horizontally Layered Sites," Earthquake Engineering Research Center, University of California, Berkeley, Berkeley, CA.

Wolf JP (1985), *Dynamic Soil-Structure Interaction*, New Jersey: Prentice Hall.

Wolf JP (1988), *Soil-Structure Interaction Analysis in Time Domain*, New Jersey: Prentice Hall.

Yoshimura C, Bielak J and Hisada Y (2003), "Domain Reduction Method for Three-Dimensional Earthquake Modeling in Localized Regions, Part-II: Verification and Examples," *Bulletin of the Seismological Society of America*, **93**(2): 825–840.

Zienkiewicz OC, Bianic N and Shen FQ (1988), "Earthquake Input Definition and the Transmitting Boundary Condition," *Conf: Advances in Computational Non-Linear Mechanics*, Editor: St. Doltnis I, 109–138.

Zhao M, Gao ZD, Wang LT, Du XL, Huang JQ and Li Y (2017), "Obliquely Incident Earthquake for Soil-Structure Interaction in Layered Half Space," *Earthquakes and Structures*, **13**(6): 573–588

Zhao M, Wu LH, Du XL, Zhong ZL, Xu CS and Li L (2018a), "Stable High-Order Absorbing Boundary Condition Based on New Continued Fraction for Scalar Wave Propagation in Unbounded Multilayer Media," *Computer Methods in Applied Mechanics and Engineering*, **334**: 111–137.

Zhao M, Li HF, Du XL and Wang PG (2018b), "Time-Domain Stability of Artificial Boundary Condition Coupled with Finite Element for Dynamic and Wave Problems in Unbounded Media," *International Journal of Computational Methods*, **15**(3): 1850099.